Reliability evaluation based on multiple response surfaces method considering
 construction uncertainties of cable tension for a hybrid roof structure

3 Youbao Jiang, M.ASCE<sup>1</sup>, Hao Zhou<sup>2</sup>, Lei Wang<sup>3</sup>, Zhao Chen<sup>4</sup>, Teng Tang<sup>5</sup>, Sondipon

4

#### Adhikari<sup>6</sup>

Abstract: For large-span hybrid roof structures, the construction uncertainties of cable 5 tension usually have significant influences on its mechanical performance and should 6 be considered in reliability evaluation. An effective approach to quantify uncertainties 7 of cable tensions and to evaluate structural reliability is proposed to carry out the 8 studies by combining the finite element simulation with the multiple response surfaces 9 method. Taking a hybrid roof structure with cables and steel trusses as an example, the 10 main procedures on this issue are illustrated. Firstly, a finite element model is 11 established for the hybrid roof structure considering construction deviations, such as 12 the deviations of cable force between the design values and the real measured values. 13 The ultimate bearing capacity of the structure is calculated for models with and without 14 15 deviations, and the effects of construction deviations on structural bearing capacity are 16 analyzed. Then, an uncertainty model of cable tension for structural reliability

<sup>&</sup>lt;sup>1</sup>Professor, School of Civil Engineering, Changsha Univ. of Science and Technology, Changsha 410114, China. Email: youbaojiang@csust.edu.cn

<sup>&</sup>lt;sup>2</sup>Doctoral Student, School of Civil Engineering, Changsha Univ. of Science and Technology, Changsha 410114, China. E-mail: haozhou@stu.csust.edu.cn

<sup>&</sup>lt;sup>3</sup>Professor, School of Civil Engineering, Changsha Univ. of Science and Technology, Changsha 410114, China. Email: leiwang@csust.edu.cn (corresponding author)

<sup>&</sup>lt;sup>4</sup>Master, School of Civil Engineering, Changsha Univ. of Science and Technology, Changsha 410114, China; Email: 470319517@qq.com

<sup>&</sup>lt;sup>5</sup>Doctor, YueYang SanHe Investment Management of Airport Construction Co.Ltd, Yueyang 414000, China. E-mail: tang7889@163.com

<sup>&</sup>lt;sup>6</sup>Professor, College of Engineering, Swansea University, Swansea SA1 8EN, United Kingdom. E-mail: s.adhikari@swansea.ac.uk

evaluation is proposed by establishing the statistics of initial strain in a structural analysis based on the monitored deviations. With subspace division and limit state sample (or sample pair), the multiple response surfaces method is developed to solve reliability for examples with complex failure functions. It is found that the hybrid roof structure has a high reliability index about 6.76; and the uncertainties of cable tensions have a large impact on the reliability, especially the uncertainties of the upper suspension cable tensions and the back cable tensions.

Key words: hybrid roof structure; cable; steel truss; multiple response surfaces method;
reliability, uncertainty of cable tension; construction deviation.

# 26 Introduction

In recent years, large-span space structures (e.g. cable domes, shell structures) have been widely used in public buildings due to their good mechanical performance and light self-weight, such as stadiums and airports (Morino 1998; Phocas and Alexandrou. 2018; Yan et al. 2019; Wakefield 1999).

31 To be largely different from simple frame structures in mechanical performance, 32 the large-span space structures often have various structural types, e.g. foldable 33 kirigami structure (Cai et al. 2019, Zhang et al. 2020), and need complex analysis and design techniques. In order to better promote the development of large-span space 34 35 structures, several scholars have carried out significant amount of researches on tensegrity structure, which can be constructed with the largest span in theoretically. 36 Fuller (1975) firstly studied a novel structure: the tensegrity structure. However, this 37 tensegrity dome structure has not been perfectly used in engineering practice. Based on 38

Fuller's thinking, Geiger et al. (1986) studied a new structure called cable dome and 39 successfully implemented the structure in the circle roof structure of the stadium for 40 41 gymnastics and fencing games of Seoul Olympic Games in 1986. In addition, further mechanical analyses of the tensegrity structures have been carried out. For example, 42 43 Kebiche et al. (1999) discussed the geometric nonlinearity of tensegrity structure. 44 Sultan et al. (2001, 2002) studied the linear dynamics of tensegrity structure and derived the linear motion equation of tensegrity structure with arbitrary equilibrium 45 configuration, and also investigated prestressing problems of tensegrity structures. 46 47 Williamson et al. (2003) studied the requirement of initial equilibrium state of tensegrity structure. Feng (2005) carried out a comprehensive study on the structural 48 49 behaviors of tensegrity dome, and performed a prototype analysis of the first tensegrity 50 dome-Georgia dome with numerical calculation. Cai et al. (2019) investigated the effects of initial imperfections of struts on the mechanical behavior of tensegrity 51 52 structure.

53 By comparison, hybrid structures, consisting of cables and rigid structures (e.g. shell structure, arch structure, truss structure), have attracted more attentions due to the 54 55 conveniences in construction. Yasuhiko et al. (1999) proposed a structural behavior analysis method and made model tests of the hybrid structures considering the effects 56 of both prestressing and static load deformation. Jiang et al. (2016) proposed an 57 effective method to study the stiffness of inner concave cable-arch structure based on 58 force method, which has main advantages that the ratio of each deformation (such as 59 bending deformation) to the total deformation can be clearly obtained through a 60

61 simplified analysis.

For both tensegrity structure and hybrid structure, which include flexible cable 62 63 members, the nonlinear effect is very obvious. Therefore, the form finding analysis is very important for the design and construction of structures. Tibert and Pellegrino 64 (2003) as well as Juan and Tur (2008) summarized the current form finding methods 65 for tensegrity structures. Cai and Feng (2015) proposed an effective numerical form 66 finding method for regular and non-regular tensegrity structures. Zhang and Ohsaki 67 (2006) presented an improved numerical method for finding the form of tensegrity 68 69 structure, which can automatically adjust the values of the force densities to adapt to the requirement on rank deficiency. 70

As well known, the node deviations in construction have a great impact on the 71 72 structural performance. Therefore, more attentions have been paid to evaluating the effects of construction deviations on structures. For example, aiming at the tension 73 system of the crescent-shaped Yueqing Stadium in China, Deng et al. (2013, 2016) 74 75 studied the effects of cable pretension deviations on structural mechanics, which is caused by the geometric deviations (e.g. manufacturing error of component length and 76 77 installation error of anchor joint). However, a deterministic analysis is mainly involved, and quantifying the influences of construction deviation uncertainties on structural 78 reliability needs to be further carried out. 79

At present, the reliability-based design and evaluation has been widely applied in engineering practice. Many methods are proposed for reliability calculation of practical structures, which usually with implicit performance functions. Among them, the

83	surrogate model method is able to obtain relatively accurate results with a small number
84	of samples [Dubourg et al. 2013], and it is widely accepted in the field of reliability
85	analysis. It approximates the performance function to calculate the failure probability
86	by constructing a surrogate model. The commonly used surrogate model methods
87	include Kriging model [Xue et al. 2017], Polynomial Chaos Expansion (PCE) [Marelli
88	and Sudret 2018], Artificial Neural Networks (ANN) [Papadopoulos et al. 2012], and
89	Response surface method (RSM) [Jiang et al. 2015] et al. Among them, the Kriging
90	model usually has good performance in approximating local characteristics. Based on
91	this characteristic, scholars proposed many adaptive Kriging methods [Teixeira et al.
92	2020; Wang and Shafieezadeh 2019; Xiao N C et al. 2019] for structural reliability
93	analysis. However, the construction of Kriging model is relatively complex, and it is
94	very time-consuming to construct Kriging model in the case of large samples. In
95	addition, the fitting effect of Kriging model is not good for high-dimensional problems.
96	PCE model has good performance in approximating global characteristics, but it has
97	the phenomenon of "dimension curse", that is, with the increase of the dimension of
98	input variables, the computation task needed for model construction increases
99	significantly [Schobi et al. 2015]. Therefore, many scholars have proposed the
100	corresponding sparse method to overcome the "dimension curse" phenomenon.
101	RSM usually has three main forms: using polynomial basis functions, radial basis

101 RSM usually has three main forms: using polynomial basis functions, radial basis 102 functions, and spline basis functions [Teixeira et al. 2020]. Due to the compromise 103 between practicability and efficiency, polynomial basis RSM is one of the most popular 104 metamodeling technique for reliability [Guimarães et al. 2018], and many scholars have

105 studied and developed it. Ju et al. (2013) proposed an adaptive response surface method based on moving least squares method. Jiang et al. (2015, 2017) proposed an efficient 106 107 response surface method based on techniques of generation of uniform support vector, which has the advantages that it can dramatically increase the proportion of support 108 109 vectors to the whole samples and requires less samples in function fitting. Hadidi et. al 110 (2017) proposed another efficient response surface method, which can greatly reduce the number of samples by using an exponential response surface model and an 111 experimental updating technique. Moreover, the accuracy of the proposed method is 112 113 improved by judiciously selecting the location of sample points which are close to the actual limit state surface. Examples show high efficiency of this method for reliability 114 analysis of simple structures, e.g. planar truss or planar frame. However, the 115 116 conventional response surface methodology has some shortcomings in reliability analysis, especially for structures with complex and high-dimensional failure functions, 117 and it is affected by the phenomenon of "dimension curse", too [Guimarães et al. 2018]. 118 119 For large hybrid roof structures with complex mechanical behaviors and a lot of uncertainties, it is difficult to quantify the influences of these uncertainties on structural 120 121 safety. In order to solve these problems, this paper establishes an uncertainty model of cable force for the finite element structure with the measured construction deviation, 122 and proposes a reliability method based on the multi-response surface technology. 123 Combing the uncertainty model with the reliability method, the reliability index of 124 structural bearing capacity is calculated. The influence of different cables on the 125 reliability of the structure is also discussed. 126

#### 127 Structural Bearing Capacity Analysis

## 128 Introduction of Hybrid Roof Structure

A terminal building is selected, which is built in Yueyang City, China and has a long-span hybrid roof structure. The whole structure consists of three parts: steel trusses, cables, and membranes, as shown in Fig.1 and Fig.2. Because the membranes are supported by the steel trusses and cables, and used for exterior protected usage only, the steel trusses and cables are considered only in the following bearing capacity analysis, as shown in Fig.3. The truss structures are used for both main bearing trusses in the middle and towers in the sides.

It is seen that the steel trusses include: truss beam (TB), truss column (TC), truss tower (TT), truss support (TS), Steel column (SC) and so on. The cables include: upper suspension cables ( $C_U$ ), lower suspension cables ( $C_L$ ), back cables in east and west sides ( $C_E$  and  $C_W$ ), membrane-supported cables ( $C_S$ ), boundary cable ( $C_B$ ) and pendent cable ( $C_P$ ) and so on. The nominal strength of cables and steel trusses are 1670 MPa and 345 MPa respectively, and other design information is shown in Table 1 and Table 2.

- 142

143

#### **Design Model without Deviations**

Based on the above section information and structural layout, the finite element model of the HRS (hybrid roof structure) was established by using ANSYS 12.0 software, as shown in Fig.4, where the Link10 tension element is used for cables, and Beam188 element is used for steel members. There are 9359 nodes and 5390 elements in the finite element model. In the finite element model, the structural parameters of cables, e.g. pretensionsand strength, are assumed to adopt their design values, as shown in Table 1.

#### 151 Structural Model with Deviations

Because the cables often play an important role in the hybrid roof structure, their tensions should be monitored carefully during the construction. To match well with their design values, key cables are monitored in construction, as shown in Fig.5. The process of tensioning the suspension cables is shown in Fig.6.

156 It is known that the measured cable tensions are varying in the whole construction 157 steps. After the constructions of all cables and trusses finished, the measured cable 158 tensions and their design tensions as well as the errors are compared. The results are 159 shown in Table 3, where  $T_d$  and  $T_m$  denote their design value and measured value, 160 respectively.

161 It is seen that the largest error is about 20% for the  $C_{L1}$  cable. Based on the 162 measured cable tensions, the finite element model can be updated, and the structural 163 model with deviations are obtained for capacity analysis.

### 164 Comparisons of Ultimate Bearing Capacity of Two Models

When the initial prestress is applied to the cable and the ultimate bearing capacity analysis of the structure, the shape of the structure will change greatly, and the small deformation assumption will no longer applicable. In order to improve the calculation accuracy, considering the material and geometric nonlinearity, the ultimate bearing capacity of the two models is analyzed. Considering the unfavorable design load combination: cool down 24 degrees Celsius, combined with 1.2DL + 1.4SL + 0.98LL, where DL, SL and LL represent dead load, snow load and live load,
respectively[GB50009-2012].

173 For the structural model without cable tension deviations, the maximum vertical displacement is about 1.12m when the structure reaches the ultimate limit state (e.g. 174 175 the maximum bearing capacity or excessive deformation which may cause structural collapse), which occurs at the node 141 of the upper suspension cable in the middle of 176 the structure, as shown in Fig.7. However, for the structural model with cable tension 177 deviations, the 190 node has the maximum displacement when the structure under 178 179 ultimate limit state. The load-displacement curves of node 141 and node 190 are shown in Fig.8. From the nonlinear curves, it can be seen that the structural nonlinear 180 behaviors are strong obviously. The ultimate bearing capacity of the design model and 181 182 the measured model are 2.21 and 2.22 respectively, and there is little difference between them. However, the difference of ultimate deformation is large, which is 1.12 m and 183 1.29 m respectively, and the deformation increases by 15.2%. The results show that 184 185 the cable force deviation has little influence on the bearing capacity of the structure, 186 but has a great influence on the displacement of the structure under the limit state, which can not be ignored. The maximum tensile stress of the cable is 457MPa, which 187 is far less than the design strength of 1670MPa. The failures of the steel structure 188 189 dominate the failures of the structure in structural bearing capacity analysis.

# 190 Uncertainty Model of Cable Tension Forces

As mentioned earlier, the actual cable tensions are measured after the constructions finished. For some cables, the measured tensions get larger than their

design value; while for other cables, the measured tensions get smaller. However, due 193 to uncertainties in service, e.g. creep of cable and rheologic changes which may cause 194 195 the prestress loss of cables (Dai et al. 2019; Kmet and Mojdis. 2013; Kmet et al. 2007), and possible damages under long-time actions (Wang et al., 2019), the cable tensions 196 197 would present complex changes by mechanical interactions and thus become uncertain during the service period, too. If the uncertainties are not carefully considered, it may 198 lead to an overestimation of safety or even an erroneous judgment. Once the whole 199 structure fails, it will cause huge losses. 200

201 For the finite element model of structure, the pretension of cable is simulated by setting initial strain in Link 10 element. In order to consider the uncertainties of cable 202 tensions practically, the initial strain of the corresponding cable can be multiplied by 203 204 an uncertainty factor  $\gamma$  in the finite element model. It is well known that the uncertain variables such as material properties, geometric parameters and dead loads of the 205 structure will fluctuate around the mean values rather than around the nominal values 206 207 [Cheng, 2010]. Moreover, based on 30 sets of tension error data in Table 3, the mean 208 value of deviations between design tension and measured tension is calculated as about 0, indicating that the uncertainty factor  $\gamma$  is reasonable to be considered as 1.0, too. 209 Therefore, the mean value of the uncertainty factor  $\gamma$  is considered as 1.0. For the 210 211 possible maximum variation of cable tension, it is assumed to be 20%, which matches well with the maximum error between the actual tension and the designed tension 212 213 shown in Table 3. Following this assumption, the standard deviation of the uncertainty factor  $\gamma$  corresponding to the initial strain can be determined. For example, Structural 214

analysis shows that if the cable force of the upper suspension cable  $C_U$  needs to be increased by 20% from 1080kN to 1300kN, the corresponding initial strain should be increased by 30%, that is, the initial strain factor  $\gamma_1$  should be 1.3, as shown in Table 4, which is the simulated design tension in the finite element model (with a small difference from the real design tension 1000kN due to simulation errors). Let  $T_{pre}$  and  $T_{post}$  be the cable force value before and after adjusting initial strain, respectively. The error *v* between them is given by

222 
$$\nu = \frac{T_{\text{post}} \Big|_{\varepsilon'_i = \gamma_i \varepsilon_i} - T_{\text{pre}}}{T_{\text{pre}}}, i = 1, 2, 3, 4 \tag{1}$$

223 Where  $\varepsilon_i$  is the initial strain.

If the cable tension deviation is assumed to follow a normal distribution (Zhang. 224 225 2014; Cheng. 2010), and the maximum varying range is considered as the  $[\mu - 2\sigma, \mu + 2\sigma]$ ( $\mu$  means the mean value,  $\sigma$  means the standard deviation) with 95.5% confidence 226 probability, then the adjustment of initial strain leading to a variation of cable tension 227 by 20% can be assumed as  $2\sigma$  (two times of the standard deviation). For example, for 228 229 the upper suspension cable C<sub>U</sub>, the standard deviation of the initial strain factor can be determined as 0.15, and the mean value is 1.0 as mentioned earlier. Similarly, structural 230 231 analysis results show that for other cables, the initial strain factor should be adjusted to  $\gamma_2 = 1.4$ ,  $\gamma_3 = 1.5$ , and  $\gamma_4 = 1.5$ , respectively, if the cable force  $T_{\text{post}}$  is increased by about 232 233 20%. To sum up, the required initial strain factors of cables and the corresponding increases of tensions are shown in Table 5. 234

Based on the data, the statistics for uncertainties of cable tension is obtained andshown in Table 6. It is used for the following reliability evaluations.

#### 237 Reliability Method based on Multiple Response Surfaces Techniques

# 238 Multiple Response Surfaces for Function Fitting

As mentioned earlier, the conventional response surface methods often use the samples not on the limit state surface, and select a single response surface model to carry out function fitting for reliability analysis of large complex structures, which possibly causes inaccurate function fitting results. Therefore, this paper develops the limit state samples and multiple response surfaces based on subspace division techniques to carry out function fitting.

245 Generally, both the number and distributions of sample points are important 246 factors affecting the function fitting accuracy. To obtain a uniform distribution of samples, the uniform design is applied widely with a uniform design table. The samples 247 produced by the uniform design method are relatively independent and uniform, 248 compared with those produced by other methods. Therefore, the uniform design 249 method is suitable to be used to generate initial sample points for acquisition of limit 250 251 state samples. If the random variables are given, the uniform design is carried out by selecting a uniform table  $U_n(q^m)$  firstly, where n is the number of experiments, and m 252 253 is the maximum number of variables, and q is the number of levels of each variable. For a random variable in physical space, it can be transformed into a standard normal 254 variable by the Rosenblatt transformation [Rosenblatt. 1952]. Herein, to simplify the 255 introduction of failure function fitting, it starts with the assumption that all random 256 257 variables are standard normal variables. The initial uniform samples in the standard normal space are obtained according to Eq. (2). 258

259 
$$x_{ij} = \left[\frac{2(u_{ij} - 1)}{q - 1} - 1\right]\lambda$$
 (2)

where  $u_{ij}$  is an element of the selected uniform table;  $x_{ij}$  is the corresponding element in the standard normal space;  $\lambda$  is a parameter for the possible distribution range of samples and is generally taken as 3.0, and the corresponding confidence probability is 99.7%. Then, use Eq. (3) to transform all initial uniform samples in the standard normal space *X* into those in the actual space *Y*.

265 
$$Y_i = F_{Y_i}^{-1}[\Phi(X_i)]$$
(3)

where  $F^{-1}()$  and  $\Phi(\cdot)$  are the inverse function of the cumulative distribution function of variable  $Y_i$  and the cumulative distribution function of the standard normal variable  $X_i$ , respectively. With the sample points in the *Y* space, the finite element model is built and a deterministic structural failure analysis is carried out, and the ultimate load  $F_{\text{lim}}$ is obtained. Then, combine the ultimate load with other resistance variables to obtain a limit state samples in the *Y* space. Finally, the limit state samples in the *X* space is obtained with Eq. (4).

273

$$X_{i} = \Phi^{-1}[F_{Y_{i}}(Y_{i})]$$
(4)

Due to complex structural properties, the real limit state surface is quite complex, too. For this sake, the whole limit state surfaces can be divided into multiple subsurfaces to obtain an accurate approximation. As well known, the closer the point on the limit state surface is to the origin in the standard normal space, the greater the influence on the failure probability. Therefore, it is necessary to pay attention to the point closest to the origin. If  $X_0$  is assumed as the closest sample point to the origin among all sample points, then an inner product coefficient of  $X_0$  and  $X_i$  are calculated by Eq. (5), and the total space can be divided into multiple subspaces for function fitting
according to the values of this coefficient.

283 
$$\rho_0(i) = (X_0 \cdot X_i) / ||X_0|| / ||X_i|| \quad i=1, 2, ..., N$$
(5)

where *N* is the number of the sample points.

The quadratic polynomial without cross terms is usually selected to consider the nonlinear characteristics of the complex failure function for function fitting. If limit state sample points are used, then it is expressed as

288 
$$\overline{g}(X) = a + \sum_{i=1}^{m} b_i X_i + \sum_{i=1}^{m} c_i X_i^2 = 0 \quad i=1, 2, ..., m$$
 (6)

where a,  $b_i$  and  $c_i$  are the fitting coefficients, m is the number of variables; and a can be taken a value as 1.0 for limit state sample points.

For all sample points, sort the values of  $\rho_0(i)$ , and select *s* representative values to divide the inner product coefficient into *s* ranges  $[\rho_0(l), \rho_0(l-1)]$  (l=1, 2, ..., s), which satisfy that  $1=\rho_0(1) \ge \rho_0(2) \ge \rho_0(3) \ge ... \ge \rho_0(s)$ . Within any range, the corresponding number of sample points is selected as 2m to satisfy that the fitting coefficients can be determined properly. Then, the whole space can be divided into *s* subspaces:  $\Omega_1, ..., \Omega_s$ , as shown in Figure 9, The response surface fitting is carried out in each subspace, and *s* response surfaces are obtained.

To combine with support vector machine techniques in function fitting, pairs of samples (safe samples and failure samples) instead of limit state samples can also be used. It is reported by Jiang et al.(2017) that the safe sample and failure sample can be generated by the safety load  $F_{l-1}$  and the failure load  $F_l$  calculated with Eq. (7) for each pair of samples, respectively, where  $\omega$  is a precision parameter and usually  $\omega$ =0.05.

$$F_{l-1} = (1-\omega)F_{\rm lim} \tag{7a}$$

304

$$F_l = (1+\omega)F_{\rm lim} \tag{7b}$$

#### 305 *Reliability Calculation Steps*

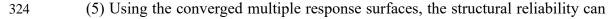
306 Using the limit state samples or sample pairs, the reliability can be calculated with307 the multiple response surface techniques by the following steps:

308 (1) With the given random variables, select a suitable uniform table to generate 309 initial uniform samples. Use Eqs. (2) to obtain the initial uniform samples in the 310 standard norm space.

(2) Combine Eqs. (3-4) with structural failure analysis techniques to obtain the
 corresponding limit state samples in the standard normal space.

(3) Use the initial limit state samples (or sample pairs) to divide the whole space
into *s* subspaces, and obtain *s* response surfaces. The principle of subspace division is
to ensure that the function fitting with the samples (or sample pairs) in each subspace
is achieved with zero residual (or with correct classification).

(4) Use the conventional reliability method (e.g. the first order reliability method) to solve the checking points for the obtained response surfaces. The function call (e.g. finite element analysis) is executed to check whether the obtained checking points are on the limit state surface. If it is not on the limit state surface, then *s* limit state samples (or sample pairs) are generated based on the ways above in step (2), and added to the current set of samples for iterative calculations. If it is on the limit state surface, the iteration converges.



be calculated with the Monte Carlo simulation. The failure probability and reliability

index are given by Eqs. (8-9)

327 
$$\overline{p}_{\rm f} = \frac{1}{N} \sum_{i=1}^{N} I[G(\overline{X})_i]$$
(8)

$$\beta = -\Phi(p_f) \tag{9}$$

329 where if  $G(\overline{X})_i < 0$ ,  $I[G(\overline{X})_i] = 1$ ; if  $G(\overline{X})_i > 0$ ,  $I[G(\overline{X})_i] = 0$ .

# 330 Numerical Verification Analysis

331 Consider the following limit state equation reported by Hadidi et al. (2017).

332 
$$G(u) = 2 - u_2 - 0.1u_1^2 + 0.06u_1^3$$
(10)

333 where  $u_1$ ,  $u_2$  are standard normal random variables.

First, a uniform sample design is carried out for this example with two random variables. A uniform table with eight training samples (N1-N8) is selected and shown in Table 7. According to Eq. (2) with  $\lambda$ =3, the initial uniform samples are transformed into those in the standard normal space, as shown in Table 8.

Next, the limit state sample points are solved. Assume  $u_1$  and  $u_2$  as resistance variable and load variable, respectively. With the given limit state equation Eq. (10) and values of  $u_1$  in Table 8, the assumed limit load values of  $u_2$  are calculated and the corresponding limit state samples are obtained, as shown in Table 9.

Then, the whole space is divided into 2 subspaces with Eq. (5) by using the 8 limit state samples in Table 9, and 2 response surfaces are obtained with Eq. (6) in subspaces. The corresponding check point is solved for each obtained response surface with the first order reliability method. It is found that the 2 check points are not on the limit state surface by calling the limit state function, and 2 limit state samples are obtained by

combining the ultimate load values of  $u_1$  with resistance values of  $u_2$  corresponding to 347 these 2 check points. Add these 2 limit state samples to update the current total sample 348 349 points for iterations of response surface fitting. Finally, the fitting is converged after 4 iterations, and 16 limit state sample points is obtained in total. The whole space is 350 351 divided into 4 subspaces, and there are 4 limit state samples in each subspace for zero residual fitting, and 4 response surfaces (RS1-RS4) are obtained, too. Because the limit 352 sate samples are used, which satisfy that performance function equals zero, the 353 354 coefficient a is assumed as a=1.0. The other coefficients of each converged response 355 surface are given in Table 10. Using these coefficients, the response surface equation can be expressed explicitly in each subspace. The obtained response surfaces are drawn 356 and compared with the real limit state surface, as shown in Fig.10. 357

From Fig.10, it can be seen that the fitted failure equation approximates the real limit state equation quite closely in each subspace. Moreover, with the fitted response surface equation, the reliability results are calculated by Monte Carlo simulation, as shown in Table 11. From the comparison of reliability results, it can be seen that the proposed method has a better accuracy and efficiency in reliability analysis.

363 Structural Reliability Analysis

#### 364 Reliability Evaluation using Multiple Response Surfaces Methodology

For this hybrid roof structure, 8 random variables are considered and their statistics are shown in Table 12, which are given in (Zhang, 2001). The reliability evaluation of bearing capacity is performed by using the multiple response surfaces (MRS) method. The main steps are as follows. 369 (1) Generation of initial uniform samples

370	As mentioned earlier, there are 8 random variables, and a uniform design with 64
371	levels is considered. The uniform design table $U_{64}(64^8)$ is selected. Taking $\lambda=3.0$ , the
372	range of variable is obtained as [-3.0, 3.0] with Eq. (2) for each initial sample point in
373	the standard normal space. The initial samples in the space $Y$ are determined by Eq. (3).
374	(2) acquisition of limit load for initial samples
375	Considering the material and geometric nonlinearity, the ultimate bearing capacity
376	of the two models is analyzed. The load combination is shown in section 1.4. Through
377	the finite element simulation by setting 500 load steps, the deterministic structural
378	failure analysis is performed to solve the limit load corresponding to each initial sample
379	points in the space <i>Y</i> , as shown in Table 13.
380	(3) fitting of multiple response surfaces
381	Based on Eq. (7), 64 groups of initial sample pairs, that is 128 sample points, are
382	obtained accordingly. Then, these sample points are transformed into those in the
383	standard normal space with Eq. (4), as shown in Table 14, where the words "S" and "F"

denote the safe sample point and failure sample point corresponding to safe and failureloads, respectively.

Among the sample points above, N7S can be determined as the closest sample point to the origin. The inner product coefficients between each sample point vector and N7S sample point vector are calculated according to Eq. (5). Then, the total space is divided into 4 subspaces based on the inner product coefficients.

390 Using the multiple response surfaces method, 4 response surfaces can be obtained

391 in the four subspaces. Then the checking points YSD1, YSD2, YSD3 and YSD4 corresponding to each response surface can be obtained, too, as shown in Table 15. 392 393 Transforming YSD1, YSD2, YSD3 and YSD4 to those in the space Y, it is found that the 4 transformed checking points are not on the real limit state surface with finite 394 395 element analysis. An iterative calculation is needed for reliability evaluation. Four new sample pairs in the standard normal space are obtained with such 4 transformed 396 checking points and the limit loads. The initial sample points are updated by adding the 397 new sample pairs, and 68 pairs of sample points, namely 136 sample points, are 398 399 obtained to divide the subspace and to perform response surface fitting again.

400 After 4 iterative steps, the obtained 4 checking points have been accurately located 401 on the real limit state surface, as shown in Table 16, thus the iterative fitting stops. A 402 total of 170 sample points including 4 real checking points are obtained. The reliability 403 indexes of 4 response surfaces in iteration are shown in Fig.11.

#### 404 Summary on Reliability Results

From Table 16, it can be seen that the uncertainties of cable tensions, especially the tensions of the upper suspension cables  $C_U$  (corresponding to  $x_5$  variables) and back cables  $C_W$  and  $C_E$  (corresponding  $x_7$ ,  $x_8$  variables), which contribute most to reliability index, have stronger impacts on reliability than other uncertainty variables. Thus special attentions should be paid to them in the construction and service periods.

410 According to the 4 converged response surfaces and Monte Carlo method, the 411 system failure probability is calculated as  $P_{\rm f}$ =6.8996e-12, and the corresponding 412 reliability index is 6.76. It indicates that the reliability level of the ultimate bearing 413 capacity is high for the structural model with uncertainties of cable tensions.

#### 414 Conclusion

This paper proposes a practical model of the uncertainties of cable forces for large hybrid roof structures and studies the influence of the uncertainties on the structure safety. In addition, an advanced multi-response surface method is studied and applied to reliability evaluation. The main conclusions are as follows:

(1) The multiple response surfaces method can be well applied to the reliability
analysis of both example with nonlinear failure function and hybrid roof structure with
a strong nonlinear mechanical behavior in loading process. By using this method, the
reliability index of the structure considering the uncertainty of cable tensions is
calculated as 6.76, which is of a high safety level.

424 (2) By multiplying the initial strain of the cable by the uncertain factors, which
425 are determined by errors between the measured cable tensions and the designed cable
426 tensions, the uncertainties of cable tension can be established conveniently in the finite
427 element model.

(3) For the hybrid roof structure composed of cables and trusses, the construction deviation will lead to a maximum difference as large as 20.06% between the actual tension of cables and the design tension. The maximum nodal displacement of the structure model without construction deviation is less than that of the structure model with construction deviation under the limit state, and the error is about 15.2%.

(4)The construction uncertainties of cable tensions have a strong impact on thereliability of the hybrid roof structure, especially the tensions of the upper suspension

435 cables and back cables. Thus, special attention should be paid to them in the436 construction and service periods.

This study shows that the construction uncertainties in hybrid roof structure do have an impact on structural mechanical performance, especially the stiffness. The positive aspect of this paper is that the proposed multi-response surface method can realize a reliability evaluation efficiently for such structure with a large number of uncertainties. To sum up, the proposed method in this paper can be widely used in the reliability evaluation for large structures with complex mechanical behaviors, which is very beneficial to evaluate the reliability for the practical structures.

444 Data Availability Statements

All data, models, and code generated or used during the study appear in thesubmitted article.

#### 447 Acknowledgement

The research is supported by the National Natural Science Foundation of China (Grant No. 51678072), National Key Research and Development Program of China (2019YFC1511000), the Key Discipline Foundation of Civil Engineering of Changsha University of Science and Technology (18ZDXK01). This support is gratefully acknowledged.

#### 453 **References**

454 Cai, J. G., and Feng, J. (2015). Form-finding of tensegrity structures using an 455 optimization method. *Eng. Struct.*, 104:126-132. https://doi.org/10.1016/

- 456 j.engstruct.2015.09.028.
- 457 Cai, J. G., Yang, R. G., Wang, X. Y., and Feng, J. (2019). Effect of initial imperfections
- 458 of struts on the mechanical behavior of tensegrity structures. Compos. Struct., 207: 871-
- 459 876. https://doi.org/10.1016/j.compstruct.2018.09.018.
- 460 Cai, J. G., Zhang, Q., Feng, J., and Xu, Y. X. (2019). Modeling and kinematic path
- 461 selection of retractable kirigami roof structures. Comput.-Aided Civil Infrastruct.
- 462 *Eng.*, 34:352-363. https://doi.org/10.1111/mice.12418.
- 463 Cheng, J. (2010). Determination of cable forces in cable-stayed bridges constructed
- 464 under parametric uncertainty. *Eng. Comput.*, 27(3):301-321. https://doi.org/10.1108/
  465 02644401011029907.
- 403 02044401011029907.
- 466 Dai, L. Z., Bian, H.B., Wang, L., and Michel, P. F. (2020). Prestress loss diagnostics in
- 467 pre-tensioned concrete structures with corrosive cracking. J. Struct. Eng., 146(3):
- 468 04020013. https://doi.org/10.1061/(ASCE)ST.1943-541X.0002554.
- 469 Deng, H., Zu, Y. Z., Shen, J. J., Bai, G. B., Dong, S. L., Zhang, Z. H., and Chen, L. Q.
- 470 (2013). Analysis and experiment on erection process of a crescent-shaped cable-truss
- 471 canopy structure. [in Chinese.] J. Zhejiang Univ., 47(3):488-494+527.
- 472 https://doi.org/10.3785/j.issn. 1008-973X.2013.03.013.
- 473 Deng, H., Zhang, M. R., Liu, H. C., Dong, S. L., Zhang, Z. H., and Chen, L. Q. (2016).
- 474 Numerical analysis of the pretension deviations of a novel crescent-shaped tensile
- 475 canopy structural system. Eng. Struct., 119:24-33. http://dx.doi.org/10.1016/
- 476 j.engstruct.2016.04.005.
- 477 Dubourg, V., Sudret, B., and Deheeger, F. (2013). Metamodel -based importance

- 478 sampling for structural reliability analysis[J]. Probab. Eng. Mech., 33: 47-57.
- 479 http://dx.doi.org/10.1016/j.probengmech.2013.02.002.
- 480 Feng, F. (2005). Structural behavior and design methods of Tensegrity domes. J. Constr.
- 481 *Steel. Res.*, 61(1):23-35. http://dx.doi.org/10.1016/j.jcsr.2004.06.004.
- 482 Fuller, B. R. (1975). Synergetics : explorations in the geometry of thinking. New York,
- 483 Macmillan Pub. Co.
- 484 Geiger, D. H., Stefaniuk, A., and Chen, D. (1986). The design and construction of two
- 485 cable domes for the Korean Olympics. In Osaka. Proceedings of IASS symposium.
- 486 2:265–72.
- 487 Guimarães H., Matos J. C., and Henriques A. A. (2018). An innovative adaptive sparse
- response surface method for structural reliability analysis. *Struct. Saf.*, 73:12–28.
  https://doi.org/10.1016/j.strusafe.2018.02.001
- 490 Hadidi, A., Azar, B. F., and Rafiee, A. (2017). Efficient response surface method for
- 491 high-dimensional structural reliability analysis. *Struct. Saf.*, 68:15-27.
  492 http://dx.doi.org/10.1016/j.strusafe.2017.03.006.
- Jiang, Y. B., Cao, Q., Kong, X., and Liao, G. Y. (2016). Stiffness study of inner concave
- 494 cable–arch structure based on an efficient method. *Adv. Struct. Eng.*, 19(12): 1927-1939.
- 495 http://dx.doi.org/10.1177/1369433216649394.
- 496 Jiang, Y. B., Luo, J., Liao, G. Y., Zhao, Y. L., and Zhang, J. R. (2015). An efficient
- 497 method for generation of uniform support vector and its application in structural failure
- 498 function fitting. *Struct. Saf.*, 54 :1-9. http://dx.doi.org/10.1016/j.strusafe.2014.12.004.
- Jiang, Y. B., Zhao, L. J., Beer, M., Patelli, E., Broggi, M., Luo, J., He, Y. H., and Zhang,

- J. R. (2017). Multiple response surfaces method with advanced classification of
  samples for structural failure function fitting. *Struct. Saf.*, 64:87-97.
  http://dx.doi.org/10.1016/j.strusafe.2016.10.002.
- Ju, S., Shenoi, R. A., Jiang, D., and Sobey, A. J. (2013). Multi-parameter optimization
  of lightweight composite triangular truss structure based on response surface
  methodology. *Compos. Struct.*, 97(2):107–116. http://dx.doi.org/10.1016/
  j.compstruct.2012.10.025.
- 507 Juan, S. H., and Tur, J. M. M. (2008). Tensegrity frameworks: Static analysis review.
- 508 Mech. Mach. Theory, 43(7):859-881. http://dx.doi.org/10.1016/j.mechmachtheory.
  509 2007. 06.010.
- 510 Kebiche, K., Kazi, M. N., and Motro, R. (1999). Geometrical non-linear analysis of
- 511 tensegrity systems. Eng. Struct., 21(9):864-876. http://dx.doi.org/10.1016/S0141-
- 512 0296(98) 00014-5.
- 513 Kmet, S., and Mojdis. M. (2013). Time-dependent analysis of cable domes using a
- 514 modified dynamic relaxation method and creep theory. *Comput. Struct.*, 125(1): 11–22.
- 515 http://dx.doi.org/10.1016/j.compstruc.2013.04.019.
- 516 Kmet, S., Tomko, M., and Brda, J. (2007). Time-dependent analysis and simulation-
- 517 based reliability assessment of suspended cables with rheological properties. Adv. Eng.
- 518 *Softw.*, 38(9): 561–575.c10.1016/j.advengsoft.2006.08.022.
- 519 Marelli, S., and Sudret, B. (2018). An active-learning algorithm that combines sparse
- 520 polynomial chaos expansions and bootstrap for structural reliability analysis[J]. *Struct*.
- 521 Saf., 75: 67-74. c10.1016/j.strusafe.2018.06.003.

MOHURD (Ministry of Housing and Urban-Rural Development of the People's
Republic of China). 2012. GB50009-2012 Load Code for the Design of Building
Structures. [in Chinese], Beijing: *China Building Industry Press*.

- Morino, S. (1998). Recent developments in hybrid structures in Japan—research,
  design and construction. *Eng. Struct.*, 20(4-6):336-346. http://dx.doi.org/
  10.1016/s0141-0296(97)00022-9.
- 528 Papadopoulos, V., Giovanis, D. G., Lagaros, N. D., and Papadrakakis, M. (2012).
- 529 Accelerated subset simulation with neural networks for reliability analysis[J]. Comput.
- 530 Meth. Appl. Mech. Eng., 223-224:70-80.
- 531 http://dx.doi.org/10.1016/j.cma.2012.02.013.
- 532 Phocas, M. C., and Alexandrou, K. (2018). Numerical analysis and cable activation in
- hybrid bending-active structures with multiple cables. *Eng. Struct.*, 174: 561-572.
- 534 http://dx.doi.org/10.1016/j.engstruct.2018.07.089.
- 535 Rosenblatt M. (1952). Remarks on a multivariate transformation. *Ann. Math.*
- 536 *Statistics*, 23(3):470—472. http://dx.doi.org/10.1214 / aoms / 1177729394.
- 537 Schobi R., Sudret B., and Wiart J. (2015). Polynomial-chaos-based kriging. Int. J.
- 538 Uncertain Quant.,5(2):171-193.
- 539 http://dx.doi.org/10.1615/Int.J.UncertaintyQuantification. 2015012467
- 540 Sultan, C., Corless, M., and Skelton, R. E. (2002). Linear dynamics of tensegrity
- 541 structures. Eng. Struct., 24(6):671-685. http://dx.doi.org/10.1016/s0141-
- 542 0296(01)00130-4.
- 543 Sultan, C., Corless, M., and Skelton, R. E. (2001). The prestressability problem of

- tensegrity structures: some analytical solutions. *Int. J. Solids Struct.*, 38(30):5223-5252.
- 545 http://dx.doi.org/10.1016/S0020-7683(00)00401-7.
- 546 Teixeira, R., María, N., and O'Connor, A. (2020). Adaptive approaches in metamodel-
- 547 based reliability analysis: A review[J]. Struct. Saf., 89 (2021): 102019.
- 548 https://doi.org/10.1016/j.strusafe.2020.102019.
- 549 Tibert, G., and Pellegrino, S. (2003). Review of form-finding methods for tensegrity
- 550 structures. Int. J. Space Struct., 18(4):209-223. https://doi.org/10.1260/
- 551 026635103322987940.
- 552 Wakefield, D. S. (1999). Engineering analysis of tension structures: theory and practice.
- 553 Eng. Struct., 21(8): 680-690. https://doi.org/10.1016/S0141-0296(98)00023-6.
- 554 Wang, L., Dai, L. Z., Bian, H. B., and Ma, Y. F. (2019). Concrete cracking prediction
- under combined prestress and strand corrosion. Struct. Infrastruct. Eng., 15(3): 285-
- 556 295. https://doi.org/10.1080/15732479.2018.1550519.
- 557 Wang, Z. Y., and Shafieezadeh, A. (2019). REAK: Reliability analysis through Error
- 558 rate-based adaptive Kriging[J]. *Reliab. Eng. Syst. Saf.*, 182: 33-45.
  559 https://doi.org/10.1016/j.ress.2018.10.004.
- 560 Williamson, D., Skelton, R. E., and Han, J. (2003). Equilibrium conditions of a
- tensegrity structure. *Int. J. Solids Struct.*, 40(23):6347-6367.
  https://doi.org/10.1016/S0020-7683(03)00400-1.
- 563 Xiao, N. C., Zhan, H. Y., and Yuan, K. (2020). A new reliability method for small failure
- 564 probability problems by combining the adaptive importance sampling and surrogate
- 565 models[J]. Comput. Meth. Appl. Mech. Eng., 372:113336.

- 566 https://doi.org/10.1016/j.cma.2020.113336.
- 567 Xue, G. F., Dai, H. Z., Zhang, H., and Wang, W. (2017). A new unbiased metamodel
- 568 method for efficient reliability analysis[J]. *Struct. Saf.*, 67:1-10.
  569 https://doi.org/10.1016/j.strusafe.2017.03.005.
- 570 Yan, X. Y., Yang, Y., Chen, Z. H., and Ma, Q. (2019). Mechanical properties of a hybrid
- cable dome under non-uniform snow distribution. J. Constr. Steel. Res., 153:519-532.
- 572 https://doi.org/10.1016/j.jcsr.2018.10.022.
- 573 Yasuhiko, H. G., and Wu, M. (1999). Analytical method of structural behaviors of a
- 574 hybrid structure consisting of cables and rigid structures. *Eng. Struct.*, 21(8):726-736.
- 575 https://doi.org/10.1016/S0141-0296(98)00027-3.
- 576 Zhang, J. Y., and Ohsaki, M. (2006). Adaptive force density method for form-finding
- 577 problem of tensegrity structures. Int. J. Solids Struct., 43(18):5658-5673.
- 578 https://doi.org/10.1016/j.ijsolstr.2005.10.011.
- 579 Zhang, M. (2014). Probability analysis and parameters identification of cable tested
- tension by frequency method. [in Chinese.], Master Dissertation, Harbin Institute ofTechnology.
- 582 Zhang, Q., Pan, N., Meloni, M., Lu, D., Cai, J. G., and Feng, J. (2020). Reliability
- 583 Analysis of Radially Retractable Roofs with Revolute Joint Clearances[J]. *Reliab. Eng.*
- 584 Syst. Saf., 208(2021):107401. https://doi.org/10.1016/j.ress.2020.107401.
- 585 Zhang, X. P. (2001). Reliability analysis and design for building structures. [in Chinese.]
- 586 Beijing: Science Press.

5	Q	Q
J	0	0

# Nomenclature

TB	truss beam	n		mber of experiments
TC	truss column	т	maxim	um number of variables
TT	truss tower	q		of levels of each variable
TS	truss support	$u_{ij}$	an eleme	ent of the selected uniform table
SC	Steel column	$x_{ij}$		ponding element in the ndard normal space
$C_U$	upper suspension cable	λ	-	ameter for the possible pution range of samples
$C_L$	lower suspension cable	$X_i$	a variable	e in standard normal spac
$C_E$	back cables in east side	$Y_i$	a va	riable in actual space
$\mathbf{C}_{\mathbf{W}}$	back cables in west side	F-1()		function of the cumulative ion function of variable }
$C_S$	membrane-supported cable	$\Phi(\cdot)$		ve distribution function of $A_i$
$C_B$	boundary cable	$F_{\rm lim}$		ultimate load
$C_P$	pendent cable	N	numb	er of the sample points
$D_{ m w}, N_{ m w}$	diameter and number of cables	$X_0$		esest sample point to the among all sample points
$T_{\rm d}, T_{\rm m}$	designed and measured pretensions of each cable	$ ho_0$	an inner	product coefficient of $X_0$ and $X_i$
DL, SL, LL	dead load, snow load and live load	$a, b_i, c_i$	the	e fitting coefficients
γ	Initial strain factor	$arOmega_i$		the $i_{th}$ subspace
$T_{\rm pre}, T_{\rm post}$	cable force values before and after adjusting initial strain	ω	р	recision parameter
v	cable force errors before and after adjusting initial strain	$p_f$	1	failure probability
З	initial strain	β		reliability index
$\mu$	mean value	$u_1, u_2$	standard	normal random variable
σ	standard deviation	COV	Co	efficient of variation
$U_n(q^m)$	uniform table	YSD		checking point
	Table.1 Design informa	ation of c	able struc	ture
Men	abers name $D_{\rm w}$ (mm)	)	$N_{ m w}$	Pretension (kN)
	C <sub>E</sub> 140		10	3915
	C <sub>W</sub> 140		10	4040

589

CL	120	5	2000
Cs	20	130	20
C <sub>B</sub>	30	10	80
Ср	20	45	0.1

# 590 Note: $D_{\rm w}$ and $N_{\rm w}$ denote the diameter and number of cables.

# 591

# Table.2 Design information of steel structure

Members name	position	Members section
	upper chord	650×20
TB	struts	426×12
	lower chord	180×8
	upper chord	325×12
TC	struts	140×6
	lower chord	325×10
50	west side	500×16
SC	east side	650×16
	upper chord	325×10
TS	struts	140×6
	lower chord	219×10
	Shuttle chord	850~1309×24~36
TT	struts	140×6
	lower chord	245×10

592	Note:	Cross-section	ı of memb	er: (diameter	$($ ) $\times$ (Thickness).
-----	-------	---------------	-----------	---------------	-----------------------------

593

# Table.3 Designed and measured pretensions of each cable

_			U		-			
	No.	T <sub>m</sub> (kN)	T <sub>d</sub> (kN)	Error	No.	T <sub>m</sub> (kN)	$T_{\rm d}({\rm kN})$	Error
	$C_U 1$	966	1000	-3.4%	C <sub>w</sub> 6	3423	4040	-18.03%
	$C_U 2$	913	1000	-8.7%	Cw7	3834	4040	-5.37%
	$C_U3$	875	1000	-12.5%	C <sub>W</sub> 8	3953	4040	-2.20%
	$C_{U}4$	923	1000	-7.7%	Cw9	3887	4040	-3.94%

C <sub>U</sub> 5	944	1000	-5.6%	Cw10	4229	4040	4.47%
$C_L 1$	2431	2000	21.6%	$C_E 1$	4075	3915	3.93%
C <sub>L</sub> 2	2267	2000	13.4%	$C_E 2$	3950	3915	0.89%
C <sub>L</sub> 3	2236	2000	11.8%	C <sub>E</sub> 3	3706	3915	-5.64%
C <sub>L</sub> 4	2244	2000	12.2%	$C_{E}4$	3734	3915	-4.85%
$C_L 5$	2311	2000	15.6%	C <sub>E</sub> 5	3484	3915	-12.37%
Cw1	4306	4040	6.18%	C <sub>E</sub> 6	3091	3915	-20.06%
C <sub>w</sub> 2	3716	4040	-8.72%	C <sub>E</sub> 7	3667	3915	-6.76%
Cw3	4126	4040	2.08%	C <sub>E</sub> 8	3747	3915	-4.48%
$C_W4$	3654	4040	-10.56%	C <sub>E</sub> 9	3704	3915	-5.70%
Cw5	3289	4040	-22.83%	C <sub>E</sub> 10	4066	3915	3.71%

594 Note: as mentioned earlier, C<sub>U</sub>, C<sub>L</sub>, C<sub>E</sub> and C<sub>W</sub> denote upper cable, lower cable, east side

595 cable, west side cable.

596 Table.4 Variations of cable tensions with increase of cable  $C_U$  tension by 30%

No.	$T_{\rm post}/{ m kN}$	T <sub>pre</sub> /kN	v
Cu	1300	1080	20.25%
$C_L$	1860	1990	-6.67%
$C_{\rm E}$	4170	4060	2.76%
$C_W$	4450	4350	2.24%

597

598

599

Table.5 Initial strain factors and the increases of tensions

Initial strain factor	Cable	T <sub>post</sub> /kN	T <sub>pre</sub> /kN	v
γ <sub>1=</sub> 1.3	$C_U$	1300	1080	20.25%
$\gamma_{2=}1.4$	$C_L$	2430	1990	22.16%
γ <sub>3=</sub> 1.5	$C_{E}$	4970	4060	22.46%
$\gamma_{4=}1.5$	$C_W$	5320	4350	22.14%

	Variable I		Distribu	tion	μ			σ			
		<b>γ</b> 1		Norm	al	1.0			0.15		
		<i>¥</i> 2		Norm	al		1.0 0.			0.20	
		<i>¥</i> 3		Norm	al		1.0			0.25	
		γ4		Norm	al		1.0			0.25	
			Table	e.7 Unif	form des	sign f	for the	numerica	l exampl	e	
	V	∕ariable	Ν	1 N	12	N3	N4	N5	N6	N7	N8
		$u_1$	2	,	7	8	3	6	5	1	4
_		$u_2$	3	:	5	7	8	2	4	6	8
			Table.	8 Unifoi	rm samp	oles i	n the st	andard n	ormal spa	ace	
_	Var	iable	N1	N2	N3	]	N4	N5	N6	N7	N8
	ι	$\iota_1$	-2.142	2.142	3.0	-1	.285	1.285	0.428	-3.0	-0.428
_	ι	<i>l</i> <sub>2</sub>	-1.285	0.428	2.142		3.0	-2.142	-0.428	1.285	3.0
	Table.9 Limit state sample points										
	Var	iable	N1	N2	N3		N4	N5	N6	N7	N8
	ι	$\iota_1$	-2.142	2.142	3.0	-]	1.285	1.285	0.428	-3.0	-0.428
	ı	$\iota_2$	0.950	2.131	2.720	1	.707	1.962	1.986	-0.520	1.976
			Table.10	) Fitting	coeffic	ients	of resp	oonse sur	face equa	ation	
	$b_i$	RS1	RS2	RS3	R	S4	$C_i$	RS1	RS2	RS3	RS4
_	$b_1$	0.978	0.267	0.23	5 110	5.31	$c_1$	-0.44	-0.22	0.086	13.93
	$b_2$	-1.49	-1.54	0.52	-21	.69	$c_2$	-5.94	-6.10	-0.45	-9.72

Table.11 Comparison of reliability calculation results

Method	No. of samples	$P_{\mathrm{f}}$	β
Proposed Method	16	3.43×10 <sup>-3</sup>	1.82
Hadidi et al. (2017)	24	2.17×10 <sup>-3</sup>	2.00
Monte Carlo method	106	3.32×10 <sup>-3</sup>	1.82

Table.12 Statistics of random variables										
X-space variable	Y-space variable	Actual variables	Distribution		COV	Ref.				
$x_1$	<i>y</i> 1	$D_L/D_{Ln}$ normal		1.06	0.074	[Zhang, 2001]				
<i>x</i> <sub>2</sub>	<i>y</i> 2	$S_L/S_{Ln}$	Type I largest	1.14	0.285	[Zhang, 2001]				
<i>x</i> <sub>3</sub>	<i>У</i> 3	L <sub>L</sub> /L <sub>Ln</sub>	Type I largest	0.71	0.206	[Zhang, 2001]				
<i>X</i> 4	<i>y</i> 4	fy/fyn	normal	1.09	0.070	[Zhang, 2001]				
<i>x</i> <sub>5</sub>	<i>y</i> 5	<b>γ</b> 1	normal	1.00	0.150	assume				
<i>x</i> <sub>6</sub>	<i>y</i> 6	$\gamma_2$	normal	1.00	0.200	assume				
<i>X</i> 7	ут	$\gamma_4$	normal	1.00	0.250	assume				
$x_8$	<i>y</i> 8	<i>γ</i> 3	normal	1.00	0.250	assume				

609 Note: item with subscript "n" means their nominal value.

# Table.13 Sample points in Y space and limit load factor

No.	<i>y</i> 1	<i>y</i> 2	<b>У</b> 3	<i>y</i> 4	<i>y</i> 5	<i>y</i> 6	<b>У</b> 7	<i>y</i> 8	$F_{\rm lim}$
N1	1.19	0.68	1.75	0.98	0.63	0.49	1.54	1.43	2.00
N2	0.97	1.73	1.15	1.27	1.26	1.16	1.33	0.64	2.20
N3	0.84	0.89	1.23	0.94	0.97	0.77	1.03	0.43	2.25
N4	1.15	1.57	1.39	0.90	0.69	1.34	1.29	1.36	1.50

N5	1.02	1.81	0.68	1.05	0.76	0.64	1.13	0.69	1.90
N58	0.98	0.57	0.68	1.24	1.02	0.60	1.31	1.68	3.20
N59	1.17	0.31	0.48	1.17	1.34	0.57	1.06	0.99	3.25
N60	1.11	1.70	0.39	0.92	1.08	0.55	1.68	1.13	1.65
N61	1.01	0.84	1.08	1.20	1.21	1.23	0.78	1.54	2.50
N62	1.25	1.44	0.46	1.00	0.56	0.92	0.71	0.73	1.80
N63	0.89	1.76	1.05	1.09	1.33	1.14	1.50	1.47	1.80
N64	1.18	1.49	1.11	1.06	0.99	0.90	1.66	0.30	1.70

Table 14 Sampling points in the standard normal space

No.	$x_1$	<i>x</i> <sub>2</sub>	<i>X</i> 3	<i>X</i> 4	<i>X</i> 5	<i>x</i> <sub>6</sub>	<i>X</i> 7	<i>X</i> 8
N7S	7.81	3.51	4.99	-2.72	1.15	2.44	0.32	0.04
N7F	8.71	3.64	5.13	-2.72	1.15	2.44	0.32	0.04
N28S	9.59	4.17	4.64	-1.8	-1.15	1.33	0.04	-1.33
N28F	10.56	4.31	4.78	-1.8	-1.15	1.33	0.04	-1.33
N59F	47.90	1.09	4.56	1.06	2.26	-2.16	0.23	-0.04
N59S	45.46	0.94	4.42	1.06	2.26	-2.16	0.23	-0.04
N44F	43.68	3.44	3.72	1.8	-1.89	-1.33	-1.8	1.61
N44S	41.41	3.31	3.59	1.8	-1.89	-1.33	-1.8	1.61

615 Note: Sample points have been sorted by distance from coordinate origin

61	6
----	---

Table.15 Checking points and reliability index for first iteration

No.	<i>x</i> <sub>1</sub>	<i>x</i> <sub>2</sub>	<i>x</i> <sub>3</sub>	<i>X</i> 4	<i>x</i> <sub>5</sub>	<i>x</i> <sub>6</sub>	<i>x</i> <sub>7</sub>	<i>x</i> <sub>8</sub>	β
YSD1	0.663	5.208	3.360	-3.340	0.048	-0.009	-0.17	0.049	7.077
YSD2	0.758	5.119	2.764	-3.680	0.060	-0.239	0.45	-0.30	6.953
YSD3	0.375	4.009	2.877	-3.250	0.198	0.230	-0.18	0.049	5.934
YSD4	0.564	3.966	3.547	-3.820	-0.025	-0.050	0.135	0.112	6.570

617 Note: YSD is expressed as checking point

Table.16 Check points and reliability index for the last iteration

DP	$x_1$	<i>x</i> <sub>2</sub>	<i>x</i> <sub>3</sub>	$\chi_4$	<i>x</i> <sub>5</sub>	<i>x</i> <sub>6</sub>	<i>x</i> <sub>7</sub>	$x_8$	β
YSD17	0.514	0.373	-0.101	-0.166	-3.387	0.971	5.884	2.107	7.206
YSD18	-0.18	-0.41	0.082	0.055	-3.544	0.819	5.517	2.995	7.271
YSD19	0.053	0.289	0.296	-0.244	-3.368	0.494	4.599	2.744	6.364
YSD20	0.214	0.042	-0.121	0.074	-4.011	0.627	4.070	3.465	6.722